TM-630
1100.400

Fermilab

PENETRATION OF PROMPT AND DECAY MUON COMPONENTS OF HADRONIC CASCADES THROUGH THICK SHIELDS

A. Van Ginneken

November 25, 1975

In the past calculations for the design of muon shields and related problems generally assumed that (1) all muons result from decay of pions (and possibly kaons) which (2) are produced in a thin target.[1,2] While this appears quite justified for some geometries, e.g., a short target followed by a long decay space, it is clearly not generally applicable.

As a first step towards a more realistic treatment the Monte Carlo program CASIM[3] which simulates the development of hadronic cascades has been modified to incorporate muon production and transport. This allows the target to be of any shape and composition and includes muons produced by all generations of the hadronic cascade. Two components are assumed to be produced: the usal decay muons and "prompt" muons.[4] The latter are assumed to have a production cross section equal to 10^{-4} of the pion yield everywhere. It must be emphasized that this is a highly questionable assumption and the results are perhaps best interpreted as upper limits. However prompt muon production has not as yet been sufficiently explored to introduce a more realistic source term. Because of this uncertainty separate tallies are kept for prompt and

decay muons. It must be pointed out that CASIM presently does not include muons resulting from kaon decay. However the normalization procedure used ensures an excess of pions roughly corresponding to the missing kaons.[3]

The production of the two muon components is simulated every time a pion is generated during the Monte Carlo run. This pion then represents (1) a prompt muon of identical momentum and direction but with a weight reduced by a factor 10^{-4} and also (2) a decay muon with direction and momentum randomly selected using the full decay kinematics and with a weight calculated assuming the pion travels one collision length before interacting.

The program CASIM uses the Hagedorn-Ranft (HR) model[5] to predict secondary particle production. A comparison with experiment[6] shows quite good agreement except for particles produced at large p_t ($\gtrsim$1.5GeV/c), precisely where prompt muon production is best known. To investigate whether these high p_t muons neglected by HR might not result in underestimating muon shielding requirements the program has been run with an extra source term representing the high p_t pions using a prescription based on the scaling formulae of Carey et al.[7] In addition to the two components derived from HR, separate tallies were kept of (3) high p_t ($\geq$1.5GeV/c) prompt muons and (4) muons from the decay of high p_t pions. The results show that while contribution (4) is negligible everywhere, the high p_t prompt muons are comparable in flux to the (HR) decay

muons at large radii. Both these contributions are generally much smaller than (1). The high p_t components are not included in the results presented in this note.

Transport of muons in the present calculation employs the continuous slowing down approximation. The range-energy relation[8] used includes effects of ionization, bremsstrahlung, pair production and nuclear interaction. Multiple scattering of the muons is calculated by the Monte Carlo method. Coulomb scattering is treated in the Gaussian approximation.[9] For muons above 10 GeV contributions to the scattering due to bremsstrahlung and nuclear interaction become appreciable and are included. Contributions to the scattering from pair production may be neglected at all energies. The angular distribution due to multiple bremsstrahlung and nuclear interaction are likewise assumed to be Gaussian with a mean square angle per unit distance as calculated by (or extrapolated from) Alsmiller et al.[2]

Thin and Intermediate Shields

One version of the present program calculates momentum spectra of muons penetrating through various thicknesses of a solid beam dump as a function of radius. The momentum selection of secondary particles in the hadronic cascade is gently biased towards large momenta to achieve a more uniform distribution in muon range since low-momentum particles are generally more numerous. Muon momentum spectra which are statistically valid at low and intermediate depths are readily obtained.

An example of such a spectrum appears in Fig. 1 which shows the muon momentum distribution after 5 m of iron at small radii ($r \leq 25$cm) for 1000 GeV/c incident protons. Prompt and decay muons are shown separately and it can be seen that the prompt muons begin to dominate above ~20 GeV/c. This fits in quite readily with the fact that in the present model prompt muons will begin to outweigh decay muons when the pion momentum at production exceeds about 36 GeV/c ($\tilde{=}10^4 \lambda m_\pi / ct$ where λ is the pion interaction length, m_π its mass and t its lifetime). The crossover occurs at a lower muon momentum mainly due to the 5 m of iron (8 GeV/c momentum loss) and the lower average momentum of the decay pions (by about 8 GeV/c).

An illustration of how the muon momentum spectrum varies with shield thickness and radial displacement is presented in Fig. 2 for the case of 1000 GeV/c protons incident on a solid soil shield. The spectra of all (prompt plus decay) muons are shown at each of three different depths for each of three radial regions. The statistical accuracy is seen to decline significantly with increasing depth.

More directly applicable in many problems such as dosimetry or detector background analysis are total (i.e., integrated over momentum) muon fluxes as a function of location. Figures 3-6 show such fluxes plotted vs radius at each of five different depths for steel and soil shields and for 400 GeV/c and 1000 GeV/c incident momenta. A separate graph is presented for decay muons and for all muons. The potential importance

of prompt muons in shielding design is evident from these plots. The results shown are everywhere statistically valid with only a slight deterioration at the larest depths shown. To convert the muon fluxes to dose it must be recalled that 1 muon cm^{-2} sec^{-1} is equivalent to about 0.13 mrem/hr.[10] The results shown for soil (assumed density of 2.0 g cm^{-3}) can be used to approximate concrete (density ~2.4 g cm^{-3}) by scaling by the ratio of the densities.

Thick Shields

The program used to generate results at shallow and intermediate depths is much less effective at very large depths. For the design of most biological shields and especially for those protecting the general population information is needed precisely at large depths and radii. Likewise, thick shields have applications in reducing background in bubble chambers and other detectors in neutrino physics experiments. To study such problems the program was modified by introducing a heavy bias towards creating high-energy pions and hence high-energy muons. A high-momentum cutoff (at ~1/4 of the incident momentum) avoids creating and tracking muons which will invariably be ranged out in the shield.

The same assumptions were used to transport the muons as for the thin shields. In contrast to the thin shield case fluctuations in muon energy loss may actually be quite important here. Nonetheless, results from the continuous slowing down

approximation are of sufficient interest to be shown. Previous calculations[1,2] likewise used this approximation but did not include any prompt muons and used less reliable pion production prescriptions. It should be pointed out however that at the large depths referred to here the thin target approximation is quite valid.

Figures 7-10 show the radial dependence of the fluxes at up to five large depths for Fe and soil shields and for 400 GeV/c and 1000 GeV/c incident proton momenta. Again a separate graph is shown for decay muons and all muons.

Other Geometries

Either version can be used to calculate more complicated geometries including heterogeneous materials. Fig. 11 shows an actual case analyzed for Fermilab's Proton experimental area. It contains the essential features of a muon shield designed to allow safe access to the enclosure even when beam is incident on the shield. The program predicts dose rates at various locations in the enclosure. By varying the configuration and dimension of the shield the design is optimized. Because of the size of high energy muon shields this is a worthwhile exercise in economics.

Even for quite simple shields it is desirable to study the actual geometry since the present results do not include effects such as muon ground-and sky shine. Figures 3-10 can then serve as a guide to the initial design which can then be improved by successive approximations.

Conclusion

For both thin and thick shields the present results demonstrate the possible importance of prompt muons. The simple prescription for prompt muon production used here is very likely an overestimate. Nonetheless, even with a greatly reduced production cross section their effects may still be significant in many shielding configurations. This has been demonstrated in the present work for the special case where only prompt muons with $p_t \geq 1.5$ GeV/c were included, which appears definitely to be an underestimate.

Acknowledgements

M. Awschalom and P. Gollon made useful comments on the manuscript. The interest of B. Cox in the analysis of the muon shield of the Proton experimental area stimulated the work performed for this note.

References

[1] D. Keefe and C. M. Noble, Radiation Shielding for High Energy Muons: The Case of a Cylindrically Symmetrical Shield and No Magnetic Fields, UCRL-18117(1968).

[2] R. G. Alsmiller et al., Muon Transport and the Shielding of High-Energy ($\leq$ 500 GeV) Proton Accelerators, ORNL-TM-3353(1971).

[3] A. Van Ginneken, CASIM Program to Transport Hadronic Cascades in Bulk Matter, FNAL-FN-272(1975).

[4] J. P. Boymond et al., Phys. Rev. Lett. 33, 112(1974); J. A. Appel et al., Phys. Rev. Lett. 33, 722(1974); L. B. Leipuner et al., Phys. Rev. Lett. 34, 103(1975); D. Bintinger et al., Phys. Rev. Lett. 35, 72(1975).

[5] R. Hagedorn, Suppl. Nuovo Cim. 3, 147(1965); R. Hagedorn and J. Ranft, Suppl. Nuovo Cim. 6, 169(1968).

[6] A. Van Ginneken, Comparison of Some Recent Data on p-Nucleus Interactions with the Hagedorn-Ranft Predictions, NAL-FN-260 (1974).

[7] D. C. Carey et al., Phys. Rev. Lett. 33, 327(1974).

[8] D. Theriot, Muon dE/dx and Range Tables: Preliminary Results for Shielding Materials, NAL-TM-229(1970).

[9] B. Rossi, High Energy Particles, p. 66 et seq., Prentice Hall, Englewood Cliffs, N.J.(1952).

[10] M. Awschalom, Some Radiation Safety Data. Personnel Radiation Doses, NAL-TM-213A(1972).

Figure Captions

Fig.1 Momentum distribution of prompt and decay muons emerging from a 5m thick iron shield at small radii ($\leq$25cm) for 1000 GeV/c protons incident on the shield.

Fig.2 Momentum distribution of all (prompt + decay) muons emerging from soil shields in three radial regions (0-50 cm, 100-150 cm and 200-300 cm) at depths of (a) 20m, (b) 100m and (c) 1000m, for 1000 GeV/c protons incident on the shield.

Fig.3 Muon Fluxes at shallow and intermediate depths in an iron shield vs. radius for (a) decay muons only and (b) all (prompt + decay) muons for 400 GeV/c protons incident on the shield.

Fig.4 Same as Fig.3 for 1000 GeV/c incident protons on an iron shield.

Fig.5 Same as Fig.3 for 400 GeV/c incident protons on a soil shield.

Fig.6 Same as Fig.3 for 1000 GeV/c incident protons on a soil shield.

Fig.7 Same as Fig.3 for large depths.

Fig.8 Same as Fig.4 for large depths.

Fig.9 Same as Fig.5 for large depths.

Fig.10 Same as Fig.6 for large depths.

Fig.11 Cross section of an actual geometry analyzed with the program shown here by way of example.

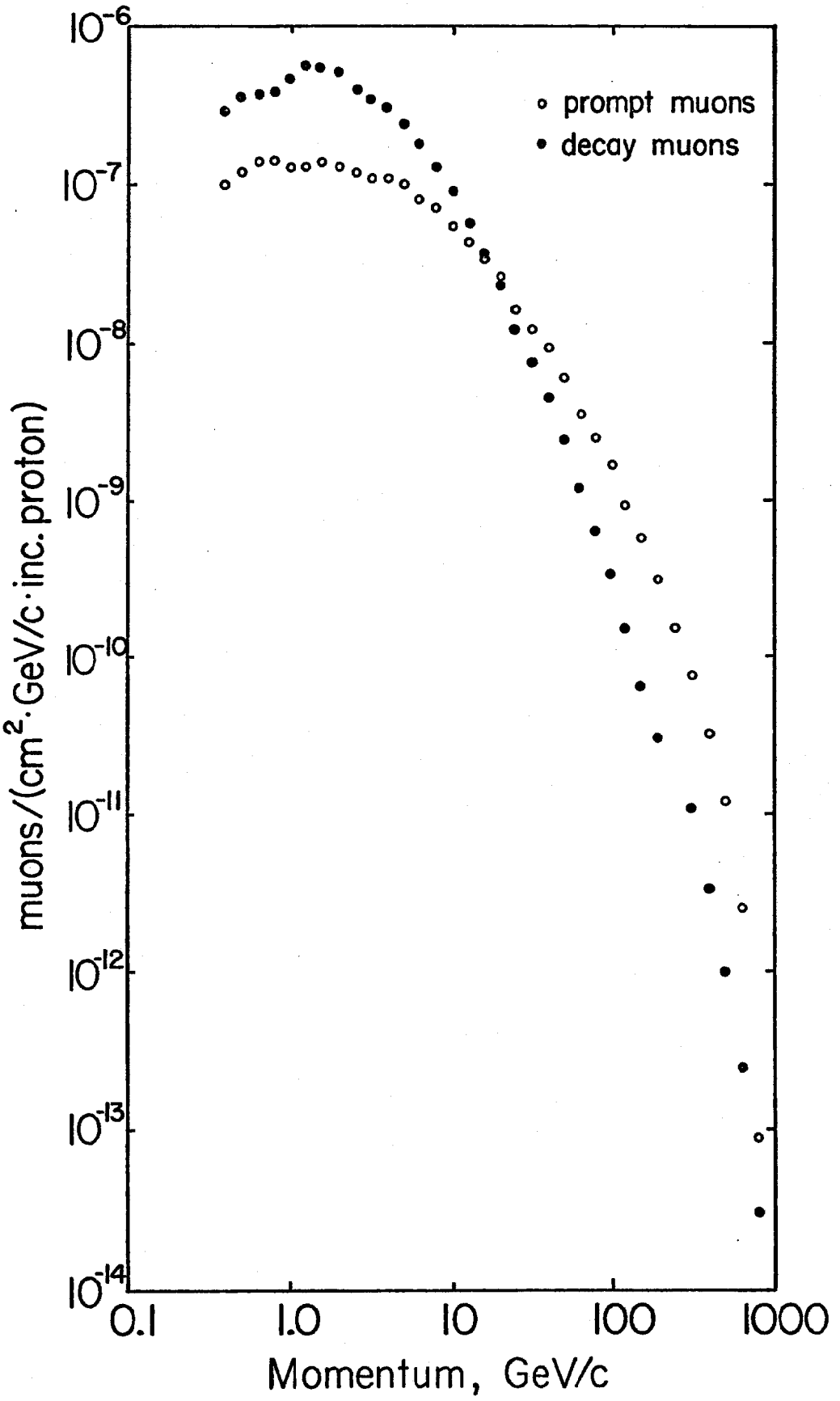
prompt muons
decay muons
muons/(cm^2·GeV/c·inc. proton)
Momentum, GeV/c
10^{-6}
10^{-7}
10^{-8}
10^{-9}
10^{-10}
10^{-11}
10^{-12}
10^{-13}
10^{-14}
0.1
1.0
10
100
1000

Fig. 1

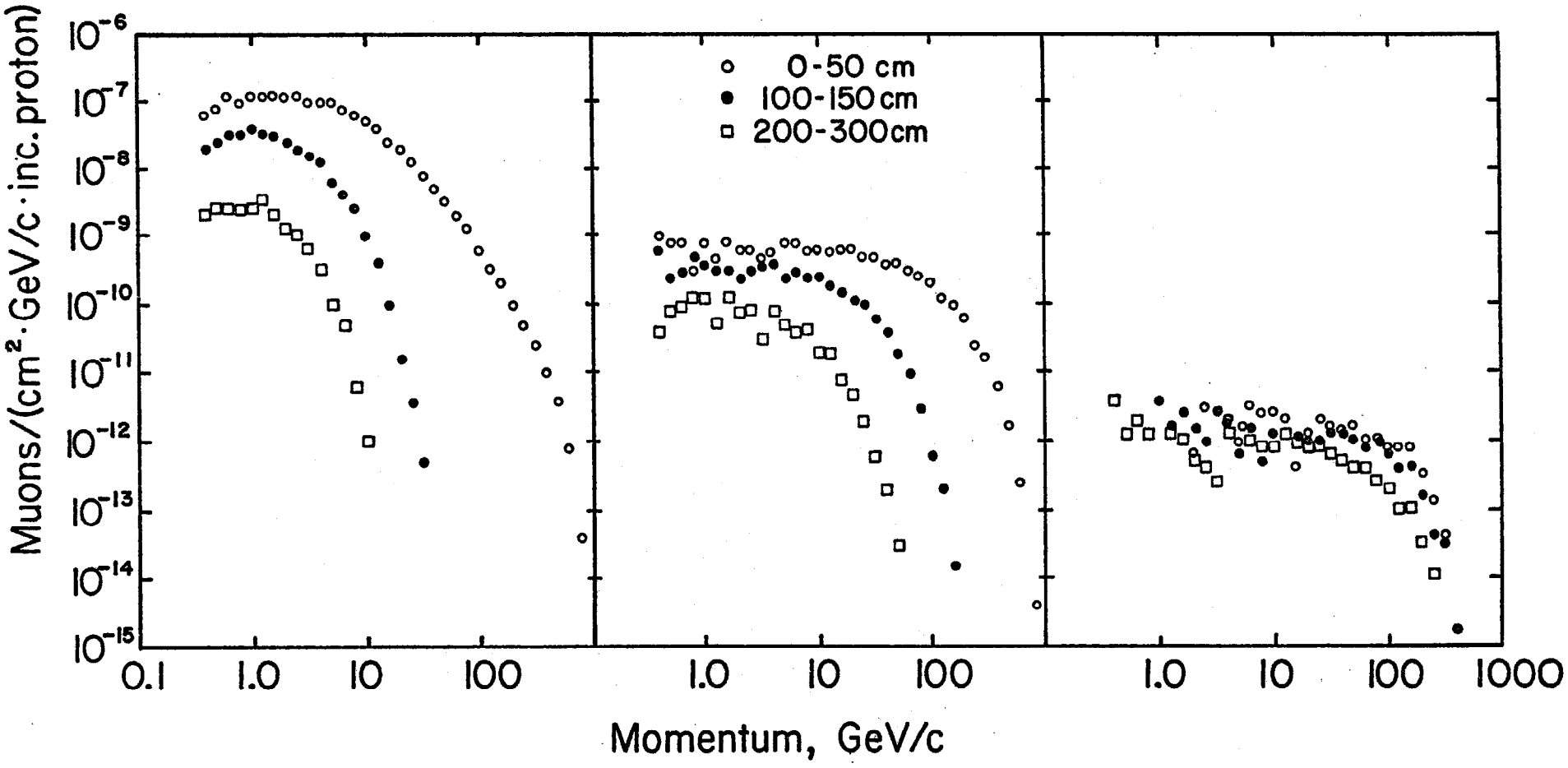

(a) (b) (c)

Fig. 2

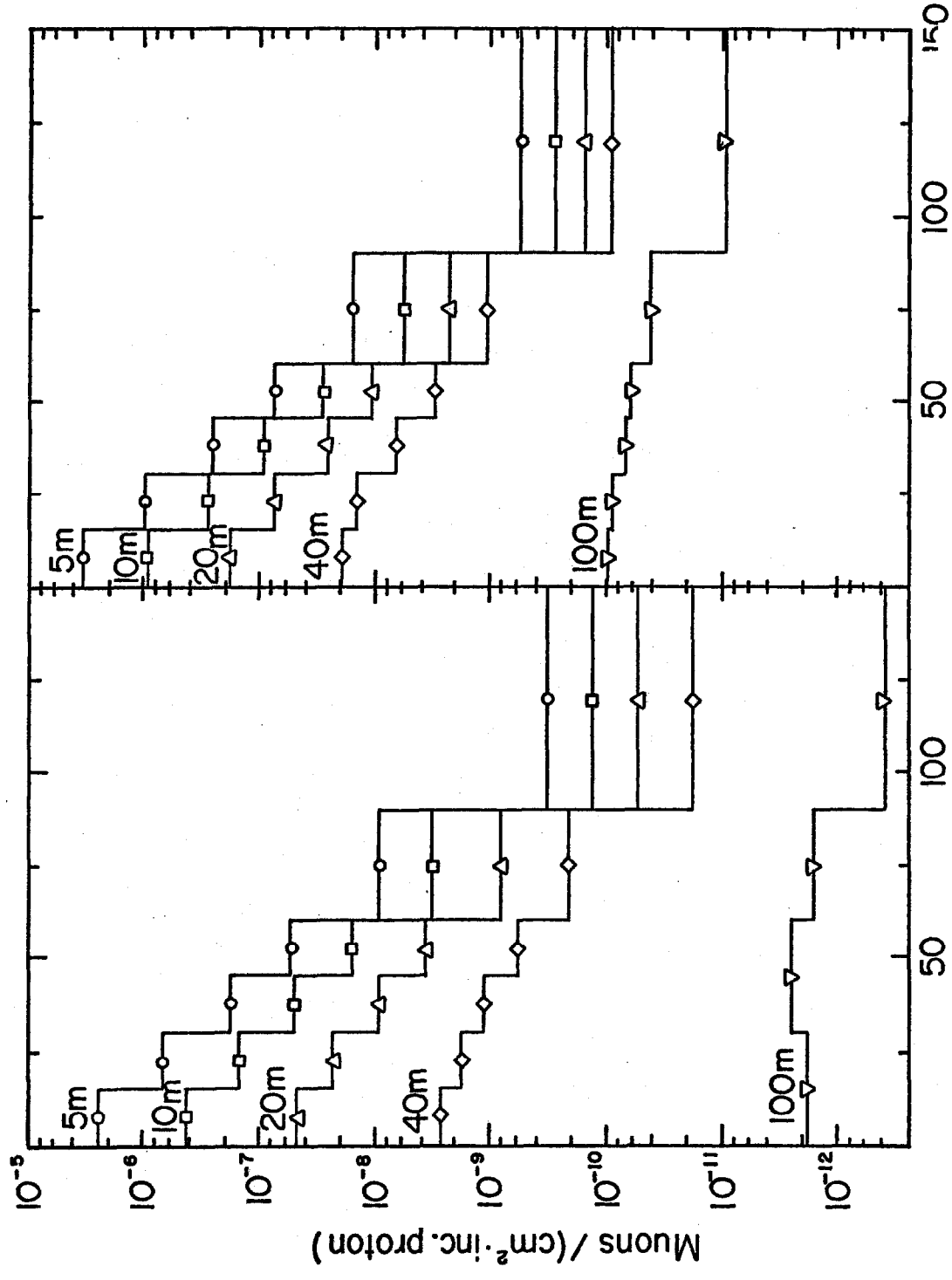
Muons /(cm^2·inc. proton)
10^{-5}
10^{-6}
10^{-7}
10^{-8}
10^{-9}
10^{-10}
10^{-11}
10^{-12}
5m
10m
20m
40m
100m
50
100
150
Radius, cm
(a)
(b)

Fig. 3

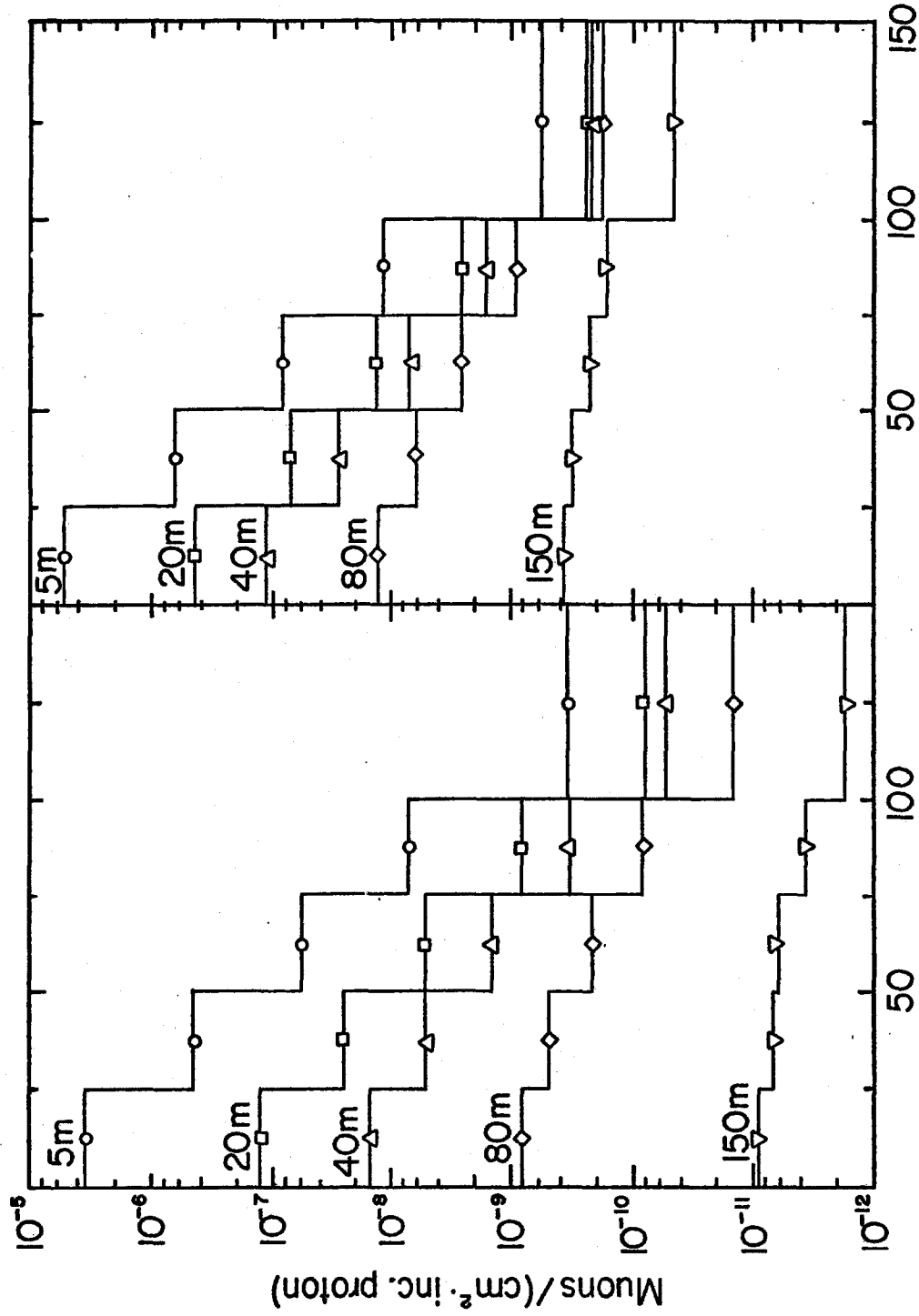
Muons/(cm^2· inc. proton)
10^{-5}
10^{-6}
10^{-7}
10^{-8}
10^{-9}
10^{-10}
10^{-11}
10^{-12}
5m
20m
40m
80m
150m
50
100
150
Radius, cm
(a)
(b)

Fig. 4

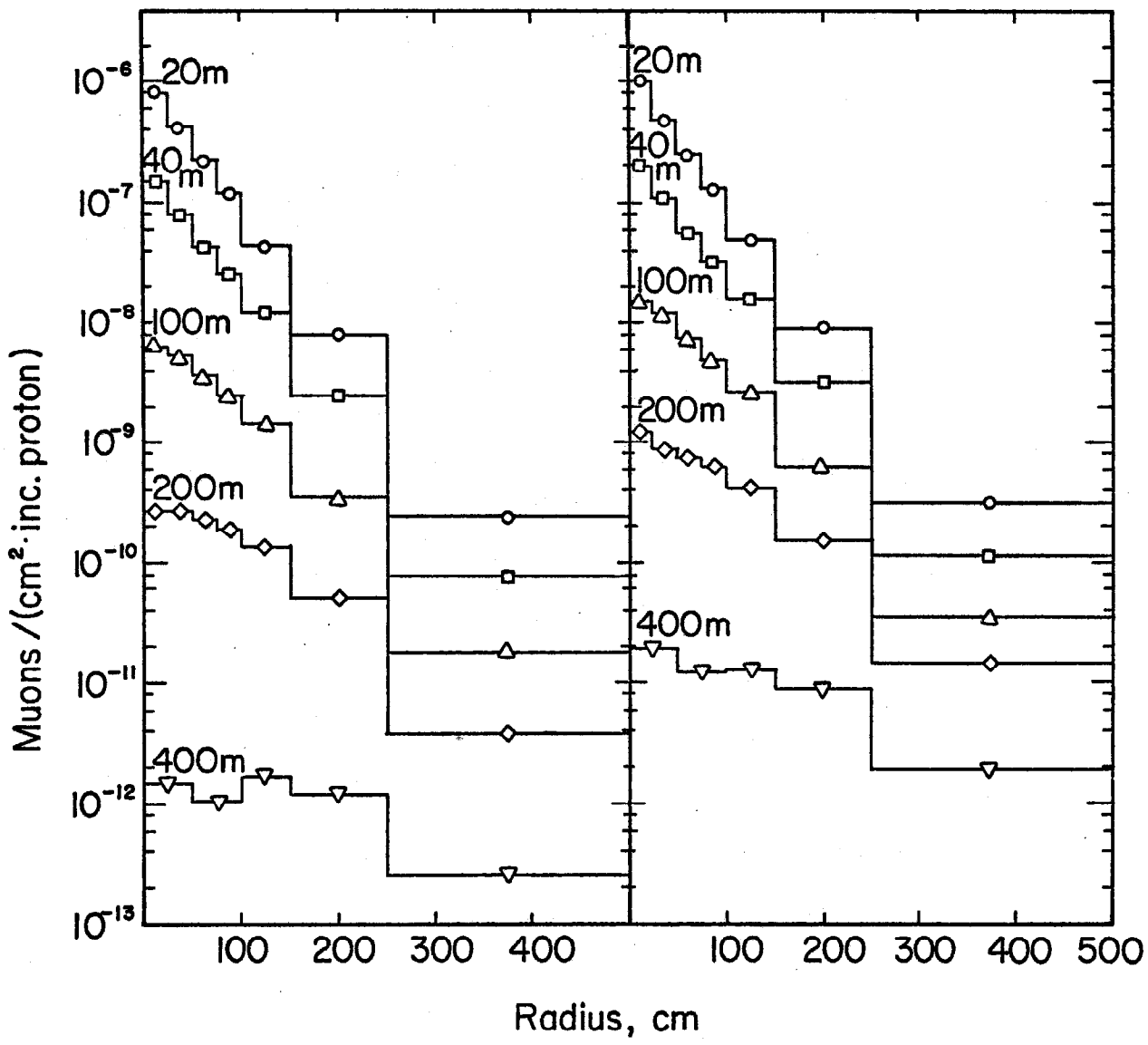
Muons /(cm²·inc. proton)
10⁻⁶
10⁻⁷
10⁻⁸
10⁻⁹
10⁻¹⁰
10⁻¹¹
10⁻¹²
10⁻¹³
20m
40m
100m
200m
400m
100
200
300
400
500
Radius, cm
(a)
(b)

Fig. 5

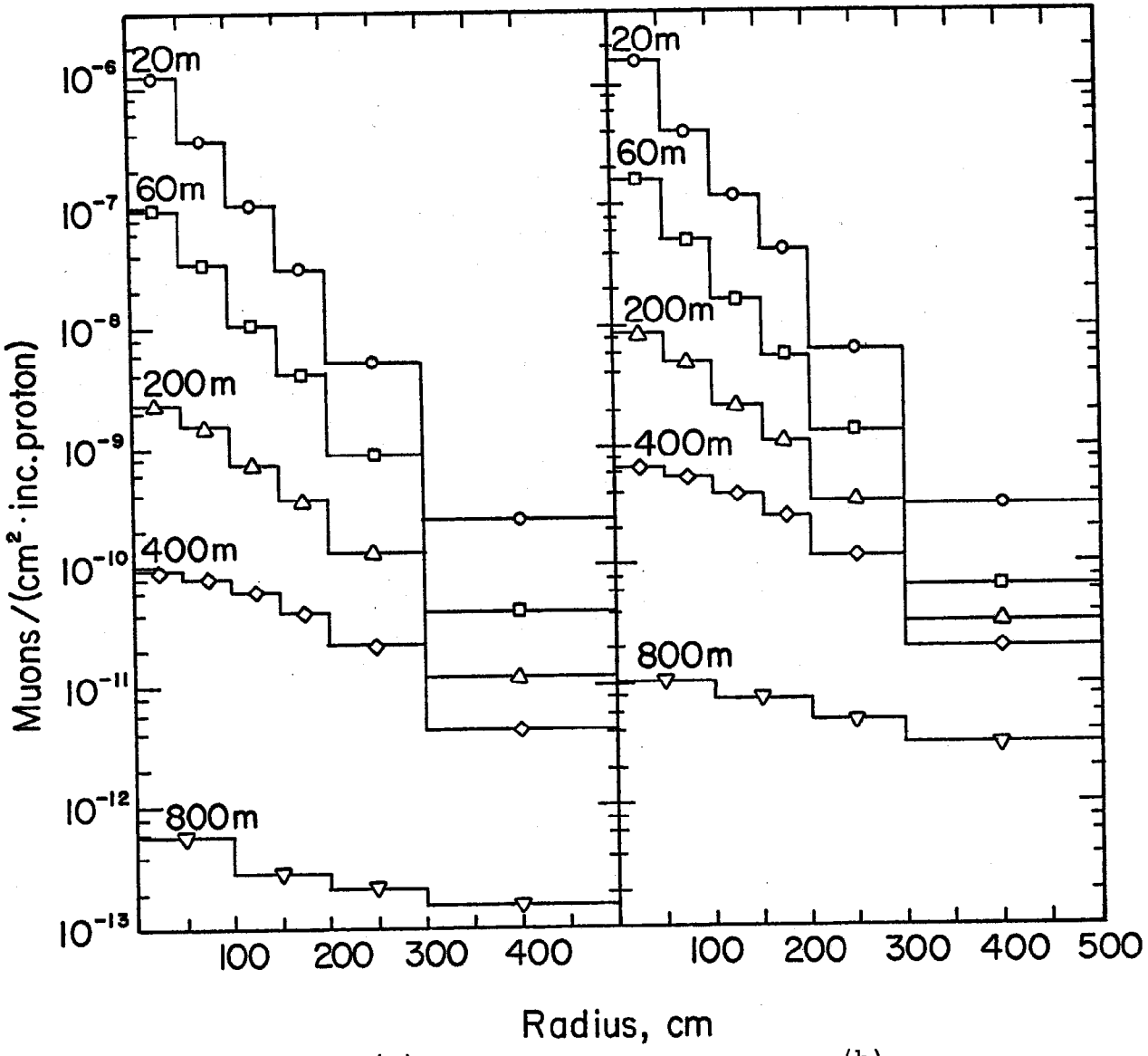
Muons/(cm² · inc.proton)
10⁻⁶
10⁻⁷
10⁻⁸
10⁻⁹
10⁻¹⁰
10⁻¹¹
10⁻¹²
10⁻¹³
20m
60m
200m
400m
800m
100
200
300
400
500
Radius, cm
(a)
(b)

Fig. 6

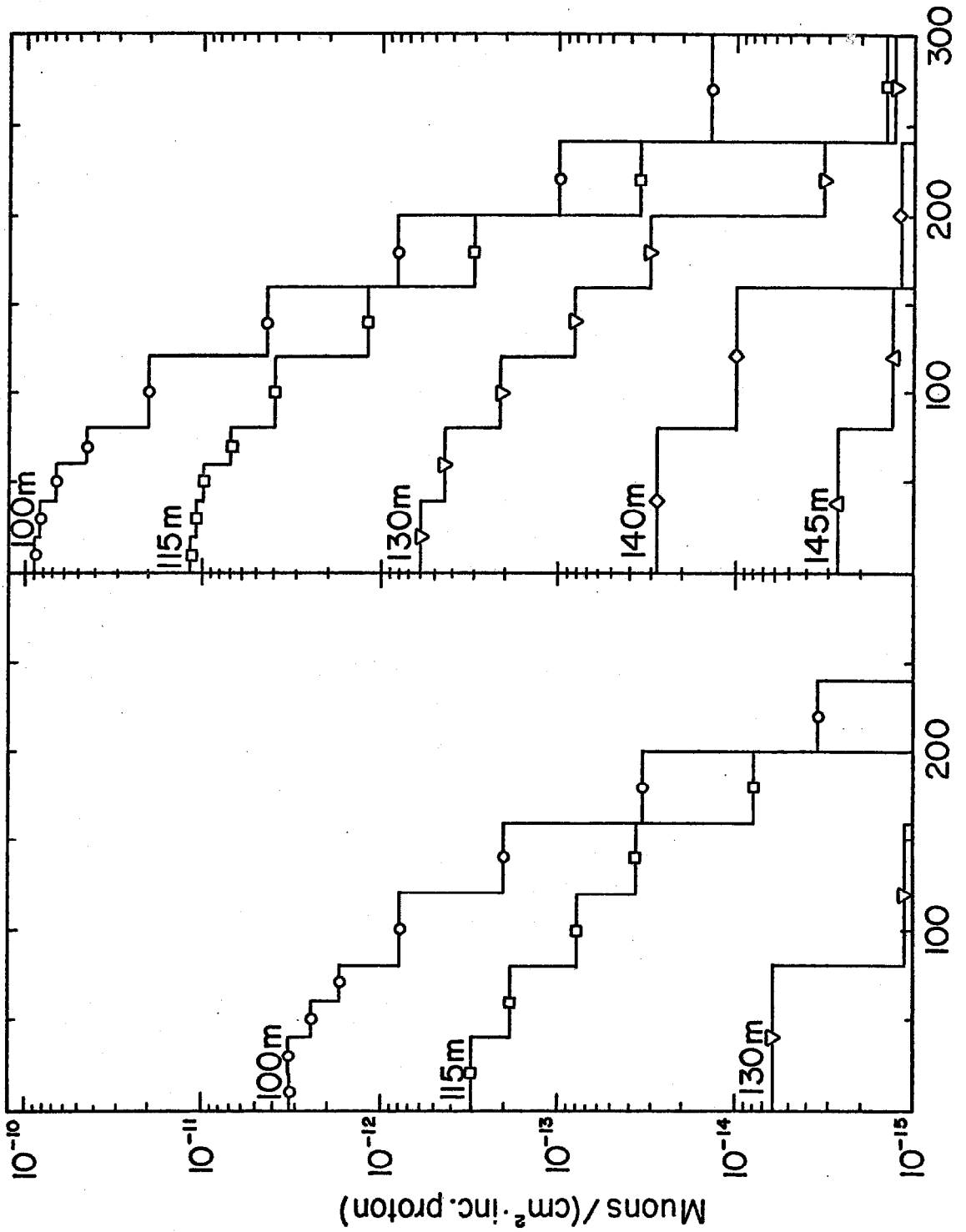
Muons / (cm² · inc. proton)
10⁻¹⁰
10⁻¹¹
10⁻¹²
10⁻¹³
10⁻¹⁴
10⁻¹⁵
100m
115m
130m
140m
145m
100
200
300
Radius, cm
(a)
(b)

Fig. 7

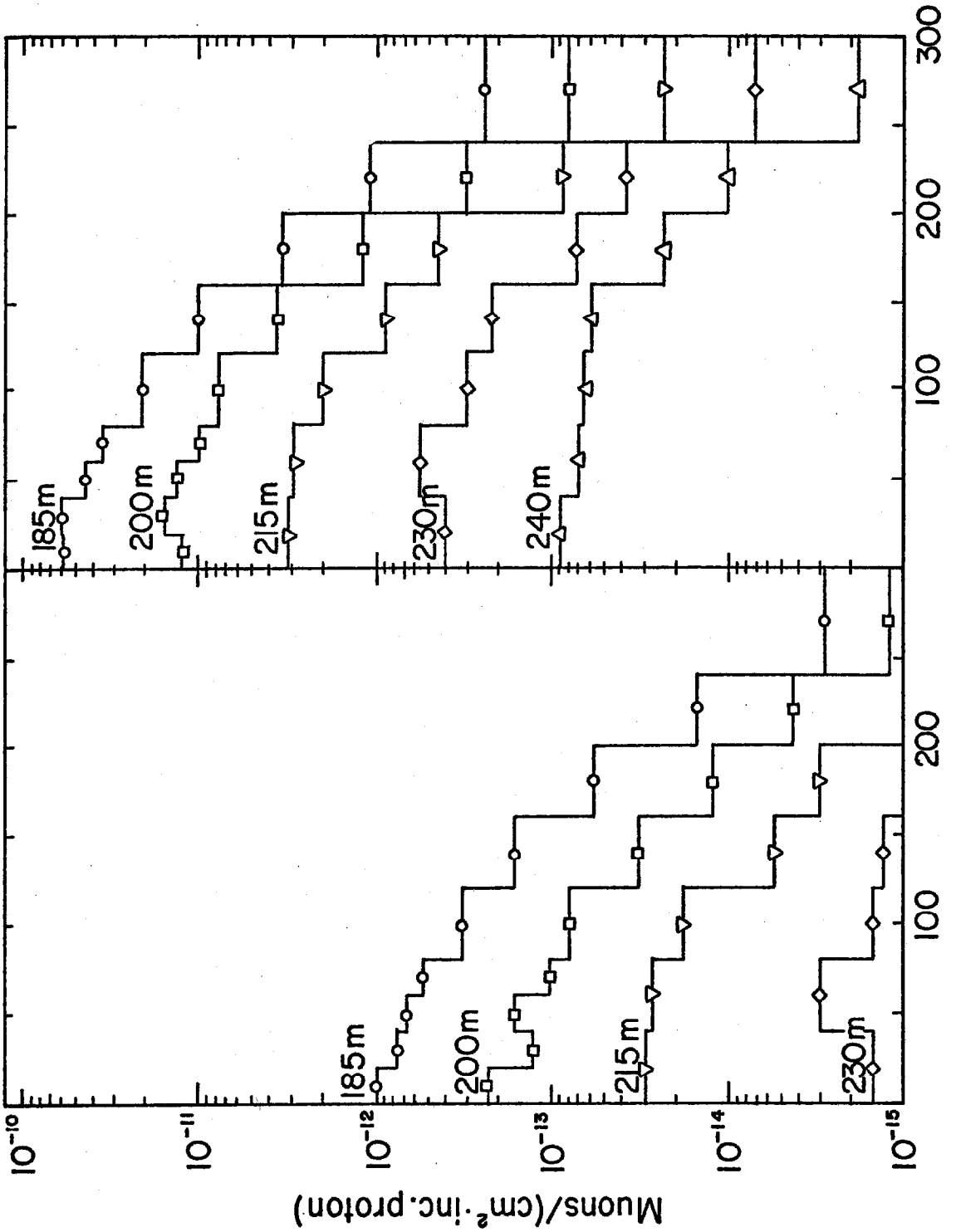
Muons/(cm^2·inc.proton)
10^{-10}
10^{-11}
10^{-12}
10^{-13}
10^{-14}
10^{-15}
185m
200m
215m
230m
240m
100
200
300
Radius, cm
(a)
(b)

Fig. 8

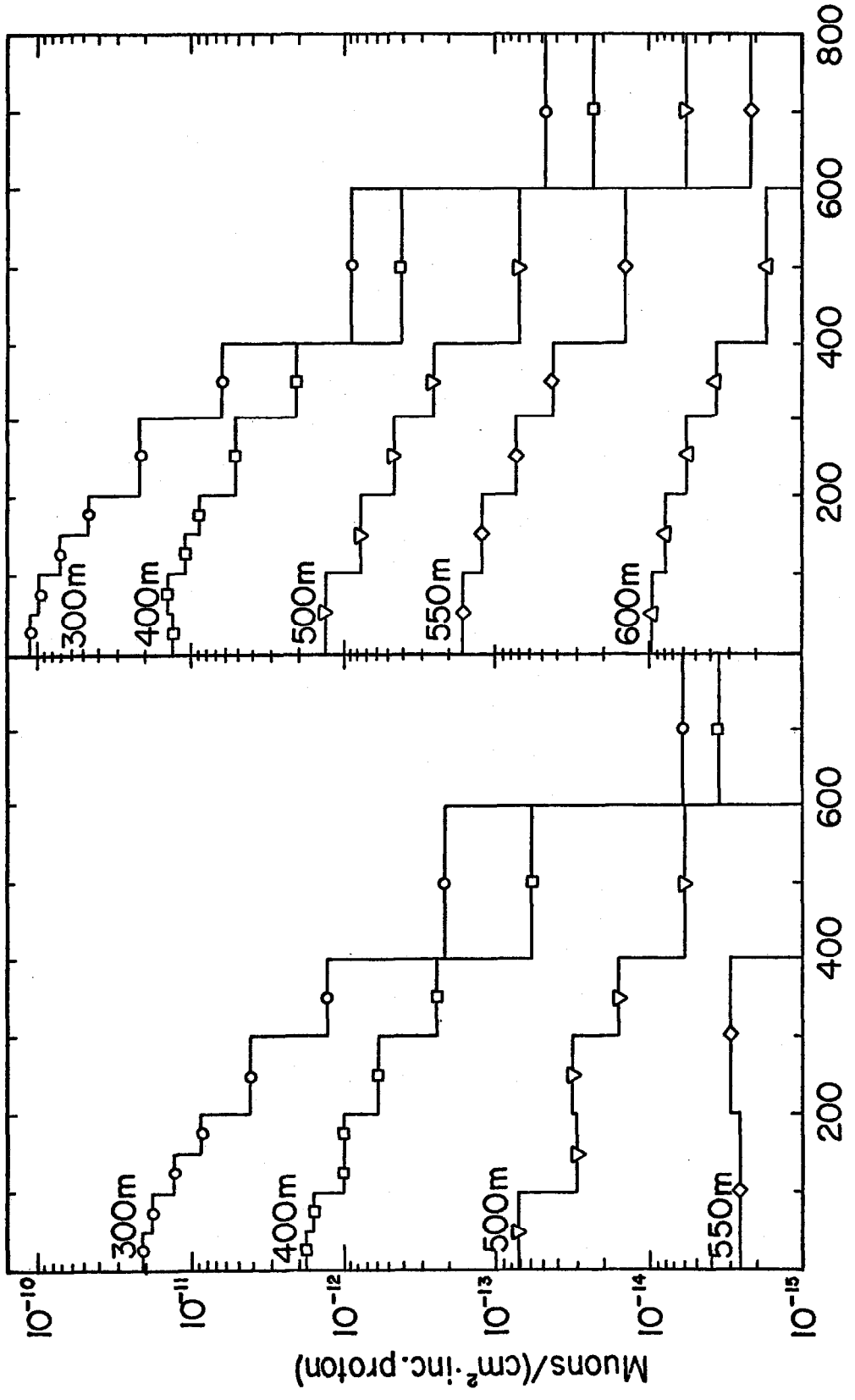
Muons/(cm²·inc.proton)
10⁻¹⁰
10⁻¹¹
10⁻¹²
10⁻¹³
10⁻¹⁴
10⁻¹⁵
300m
400m
500m
550m
600m
200
400
600
800
Radius, cm
(a)
(b)

Fig. 9

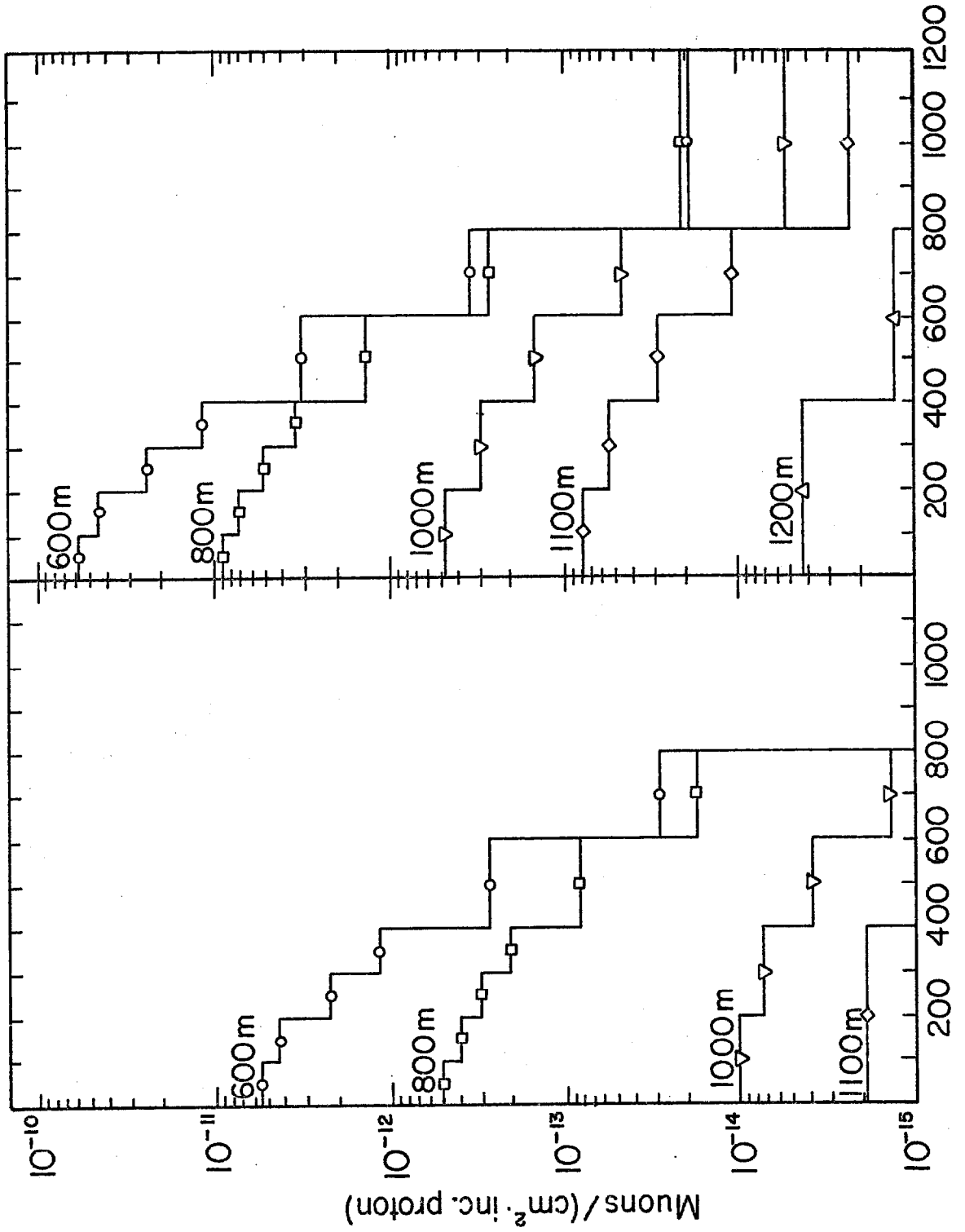
Muons / (cm² · inc. proton)
10⁻¹⁰
10⁻¹¹
10⁻¹²
10⁻¹³
10⁻¹⁴
10⁻¹⁵
600m
800m
1000m
1100m
1200m
200
400
600
800
1000
1200
Radius, cm
(a)
(b)

Fig. 10

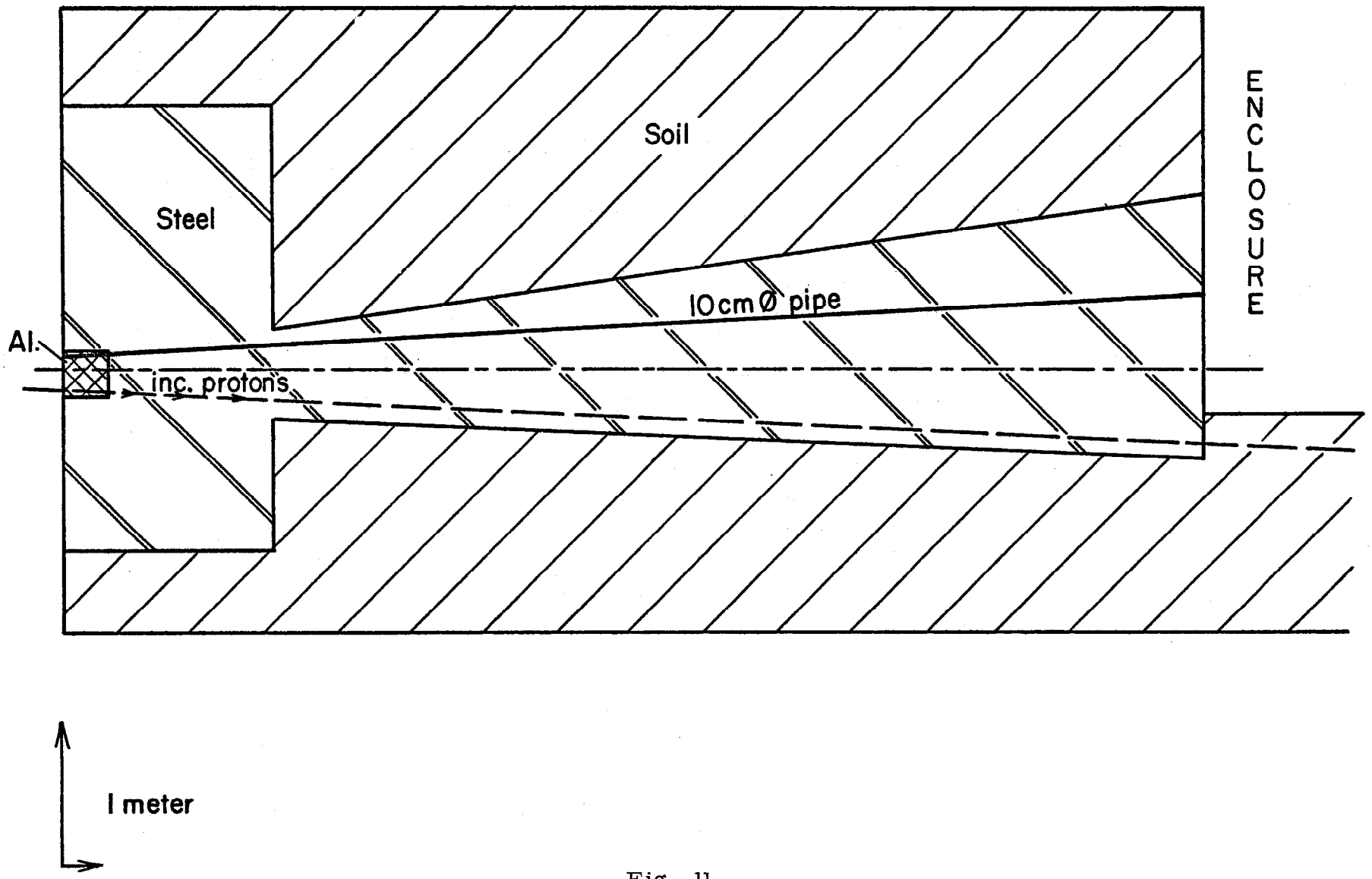

Fig. 11